J Nanostruct 15(4): 1678-1689, Autumn 2025

RESEARCH PAPER

First-Principles Investigation of H_2S Adsorption on $(ZnO)_{14}$ Nanoclusters: Electronic, Vibrational, and Topological Insights

Eateman Salah Mahdi [1], ***Uday Abdul-Reda Hussein*** [2], ***Ali Fawzi Al-Hussainy*** [3], ***Usama S. Altimari*** [4], ***Shaimaa Abd*** [5], ***Aseel M. Aljeboree*** [1], ***Ayad F. Alkaim*** [1*]

[1] *Department of Chemistry, College of Sciences for Women, University of Babylon, Iraq*

[2] *Department of Pharmaceutics, College of Pharmacy, University of Al-Ameed, Iraq*

[3] *College of Pharmacy, Ahl Al Bayt University, Kerbala, Iraq*

[4] *Department of Medical Laboratories Technology, AL-Nisour University College, Baghdad, Iraq*

[5] *Department of Medial Laborites, Al-Manara College For Medical Sciences, Maysan, Iraq*

ARTICLE INFO

Article History:
Received 07 May 2025
Accepted 27 August 2025
Published 01 October 2025

Keywords:
Atoms in Molecules (AIM)
Chemisorption
Electronic structure
Gas sensing
ZnO nanocluster

ABSTRACT

The efficient detection and capture of hazardous gases like hydrogen sulfide (H_2S) are vital for environmental monitoring and industrial safety. In this study, we perform a comprehensive theoretical analysis of H_2S adsorption on a $(ZnO)_{14}$ nanocluster using density functional theory (DFT) and time-dependent DFT (TD-DFT). Structural optimizations, frontier molecular orbital (FMO) analysis, Mulliken charge distribution, vibrational frequency calculations (FT-IR), adsorption energy, and Atoms in Molecules (AIM) topological analysis were conducted to investigate the electronic and physicochemical properties before and after gas adsorption. The adsorption energy calculations confirmed that H_2S undergoes chemisorption on the ZnO surface, with an energy of interaction indicating favorable thermodynamics. FMO analysis showed a significant reduction in the HOMO–LUMO gap from 7.94 eV (H_2S) and 0.16 eV (ZnO) to 0.43 eV for the H_2S/ZnO complex, suggesting enhanced electronic conductivity and potential sensor activity. AIM analysis revealed weak to moderate interactions between the adsorbate and the surface, with positive Laplacians ($\nabla^2\rho$) and low-to-moderate electron density (ρ) at the bond critical points, indicating partially covalent character. Importantly, the IR spectral analysis demonstrated a marked shift and broadening of characteristic H_2S vibrational modes upon adsorption. Notably, the S–H stretching modes at ~2600 cm^{-1} were either red-shifted or disappeared entirely in the H_2S/ZnO complex, while new modes corresponding to Zn–S and O–H stretching appeared in the fingerprint region, confirming strong interaction and structural reorganization. These vibrational changes validate the adsorption mechanism predicted by energy and charge analyses.

How to cite this article
Mahdi E., Hussein U., Al-Hussainy A. et al. First-Principles Investigation of H_2S Adsorption on (ZnO)14 Nanoclusters: Electronic, Vibrational, and Topological Insights. J Nanostruct, 2025; 15(4):1678-1689. DOI: 10.22052/JNS.2025.04.016

INTRODUCTION

Hydrogen sulfide (H_2S) is a highly toxic, corrosive, and odorous gas derived from various natural and anthropogenic sources which includes volcanic activity, geothermal springs, crude oil refineries, wastewater treatment facilities, and anaerobic digestion occurring in sewage and

* *Corresponding Author Email: alkaimayad@gmail.com*

animal farm houses [1, 2]. H_2S at concentrations of 10 ppm is known to cause eye irritancy and olfactory fatigue and supra 300 ppm causes accelerated asphyxiation and death [3]. Besides the direct impacts on health, the corrosion of steel pipelines, and concrete infrastructure, influenced by H_2S causes important losses in economic terms [4-6].

Semiconductor metal oxides have been widely accepted as the workhorses in the category of resistive gas sensor owing to the low cost, miniaturization, and high stability against harsh environments [7, 8]. ZnO, a II–VI semiconductor with a direct band gap of 3.3 eV and a large exciton binding energy (60 meV) is one of the most promising ones. Having a wurtzite crystal structure, it can develop rich morphologies (nanowires, nanosheets, hollow sphere, and quantum dots), wherein these morphologies offer a large number of surface sites that can interact with the target gases [7]. When reducing molecules (e.g., H2S) are adsorbed on ZnO and donate their electrons to the conduction band (CB), the sensor resistance can decrease, which can be used for the chemiresistive sensing. While many important experimental studies exist, which demonstrate ppb-level sensitivity to H_2S of ZnO films and nanowires [9], a comprehensive mechanistic picture at the atomic level is lacking, particularly for finite nanoscale clusters that differ from ideal bulk surfaces.

Density functional theory (DFT) has become a powerful tool that significantly assists in understanding gas–surface interactions and enables quantitative predictions of adsorption energies (E_ads)[10], charge flow, as well as changes in electronic and vibrational structure. In early DFT models for ZnO as an extended slab, it was found that H_2S binds selectively to the Zn-terminated (0001) surfaces with dissociative adsorption energies between −1.2 and −1.8 eV [11, 12]. But, actual sensing layers contain nanocrystalline domains which have their local coordination environments in the form of ZnO clusters. Recent theoretical investigations on (ZnO) n (n ≤ 12) clusters have revealed a size-dependent change of the band gap, work function, and Lewis acidity/basicity, which strongly affect the adsorption behaviour of gas molecules [13]. In particular, the $(ZnO)_{14}$ nanocluster has often been referred to as the smallest cluster which still maintains an important aspect of wurtzite ZnO (tetra-coordinated Zn and O centers) and at the same time is computationally affordable for high level analyses like time-dependent DFT (TD-DFT) and charge density topology studies [14, 15].

Notwithstanding these developments, there are still several shortcomings. First, the relationship between H_2S adsorption and FMOs of $(ZnO)_{14}$ nanocluster has not been investigated in a systematic way. Therefore, it is important to understand how the HOMO–LUMO gap will reduce or how new defect levels will form upon adsorption in order to correlate the electronic footprint with resistance difference. Second, there are few existing workflows that self-consistently combine various quantitative measures such as Mulliken charges, natural bond orbital (NBO) populations and Atoms-in-Molecules (AIM) metrics (ρBCP, ∇^2PBCP, and energy densities), despite such an integrated approach being essential for the discrimination between physisorption (closed-shell, weak) and chemisorption (partially covalent, strong). Third, vibrational signatures –in particular S–H stretching and bending modes– provide a complementary tool to investigate adsorption geometry, which may be compared with in-situ infrared spectroscopy, a tool rarely considered in ZnO clusters.

In this work, we aim to fill these gaps by means of a thorough DFT study of H_2S adsorption on the $(ZnO)_{14}$ nanocluster. Geometry optimizations and frequency calculations are performed at the B3LYP/6-31G(d) level which provides a good compromise between accuracy and computer time in the case of metal–oxide systems [16]. The adsorption energies are counterpoise-corrected to BSSE to avoid an overestimate of the interaction, and other possible error how to splitting of the complex into nascent fragments and increase on electron transfer from adsorbate to metallic surface. Using thermodynamic corrections (zero-point energy and thermal enthalpy/entropy terms), Gibbs free energies (ΔG_ads) at standard conditions (298 K, 1 atm) can be derived to gauge spontaneity in practical sensing environments [17].

In addition to energetics, extensive electronic analyses have been carried out. The frontier orbital energies (HOMO and LUMO) and the band gaps are determined from single-point calculations for the isolated H_2S molecule, pure $(ZnO)_{14}$ nanocluster, and the $H_2S/(ZnO)_{14}$ complex adduct. DOS and PDOS plots show orbital mixing

and channelling of charge transfer around the Fermi level. According to the TD-DFT excited-state calculations, absorption wavelengths and oscillator strengths are estimated and opto-electronic responses following gas binding have been discussed. Charge analysis by Mulliken and natural bond orbital (NBO) describes the electron trickle from H_2S into $(ZnO)_{14}$ nanocluster, the relationship type (ionic or covalent) of the Zn–S and O–S contacts is recognized by the AIM topological parameters of the bond-critical points (BCPs). It also demonstrates a blue-shift in ν(Zn–O) and a redshift for ν(S–H) modes, which indicates that the electrons have shaken from H_2S to the sites of Zn and Zn–S or O–S have been enhanced. Such computational spectra may be compared directly with FT-IR or Raman data providing an experimental validation pathway for sensor designs.

Taken together, the multi-faceted data contributes towards a consistent picture of how H_2S adsorption is understood by ZnO nanoclusters, including thermodynamics of adsorption, electronic structure modulation, electron density topology and vibrational fingerprints. Results not only inform the understanding on a fundamental level but also provide simple design principles: (i) surface Zn sites in low coordination (two or three) serve as high affinity adsorption sites; (ii) moderate reduction of the HOMO–LUMO gap (~0.4 eV) upon adsorption leads to ohmic behavior without placing the sensor in the regime of irreversible chemisorption; and (iii) AIM descriptors ρ_BCP ≈ 0.07–0.10 e Å^{-3} and positive $\nabla^2\rho$_BCP signal partially ionic Zn–S bonds, which favor reversible sensing. The knowledge can be applied to technological development of ZnO nanocluster aggregates or doped ZnO films that enable high H_2S response without sacrificing fast recovery and long term stability.

MATERIALS AND METHODS

Computational Details

All quantum-chemical calculations were performed with the Gaussian 09 program package. The geometries of H2S, $(ZnO)_{14}$ nanocluster, H_2S–$(ZnO)_{14}$ complex were optimized using DFT at B3LYP/6-31G(d) level. Relativistic effects for Zn atoms were included using the effective core potential LANL2DZ. All structures have been verified as true minima by vibrational frequency analysis which revealed no imaginary frequencies. The structure visualization and orbital graphics were carried out via the software of the GaussView 6.0.

Vibrational Frequency Analysis

The stability of the optimized geometries as well as the vibrational modes altered by the adsorption were analyzed by performing harmonic vibrational frequency calculations at the same level of theory. The calculated interaction-induced spectral shift analysis have been performed mainly for H–S stretching modes. Frequencies and IR intensities were directly taken from the Gaussian outputs and OriginPro was used to visualize data for comparisons.

Adsorption Energy and Thermodynamic Analysis

The adsorption energy (E_{ads}) of H_2S molecule on $(ZnO)_{14}$ nanocluster was computed using the expression:

$$E_{ads} = E_{complex} - (_{EZnO} + E_{H_2S})$$

Thermodynamic parameters such as Gibbs free energy (ΔG) and enthalpy change (ΔH) were calculated at 298.15 K and 1 atm from Gaussian frequency output. These quantities allowed assessment of spontaneity and thermal favorability of the adsorption process.

Electronic Structure and UV–Vis Analysis

Frontier Molecular Orbital (FMO) energies, including HOMO, LUMO, and energy gap (ΔE), were calculated for the isolated and complexed systems. Time-dependent DFT (TD-DFT) calculations were performed using the same functional and basis set, specifying NStates = 20, to simulate electronic transitions and absorption bands. The UV–Vis spectra were processed using OriginPro for peak assignment and spectral shift evaluation.

Charge Distribution and AIM Topological Analysis

Mulliken population analysis was employed to evaluate charge transfer behavior upon adsorption. To characterize bonding interactions, Atoms in Molecules (AIM) theory was applied using Multiwfn and AIMAll software. Wavefunction files (.wfn and.fchk) were generated from Gaussian outputs. Key descriptors—electron density (ρ), Laplacian ($\nabla^2\rho$), and energy densities (G, V, H)—were computed at bond critical points (BCPs) to analyze the nature of intermolecular interactions

such as Zn–S and S–O contacts.

Visualization and Plotting

Molecular orbitals, AIM bond paths, IR spectra, and HOMO–LUMO energy diagrams were visualized using GaussView, AIMAll, VMD, and OriginPro 2024. All figures were formatted at high resolution for publication standards.

RESULTS AND DISCUSSION

Frontier Molecular Orbital Analysis

We find that H_2S has a large HOMO (–6.85 eV) and a large LUMO (+1.09 eV), leading to a wide bandgap of 7.94 eV (Figs. 1 and 2). This indicates its closed-shell configuration and high kinetic stability. In contrast, the ZnO cluster has a much smaller band gap of 0.16 eV, also HOMO and LUMO almost at the Fermi energy. This reiterates the semiconducting nature of ZnO and its suitability as a reactive surface especially for electron transfer reactions. Upon complexation of H_2S, the electronic structure of the H_2S–ZnO system is significantly changed: the HOMO level moves upward to –4.69 eV and the LUMO level moves downward to –4.26 eV, which leads to a remarkably narrowed band gap of 0.43 eV. Such shifts indicate increased electronic delocalization and interaction of H_2S with ZnO, which implies a chemisorptive interface bonding.

Mulliken Charge Distribution

Mulliken atomic charge distributions (Fig. 3)

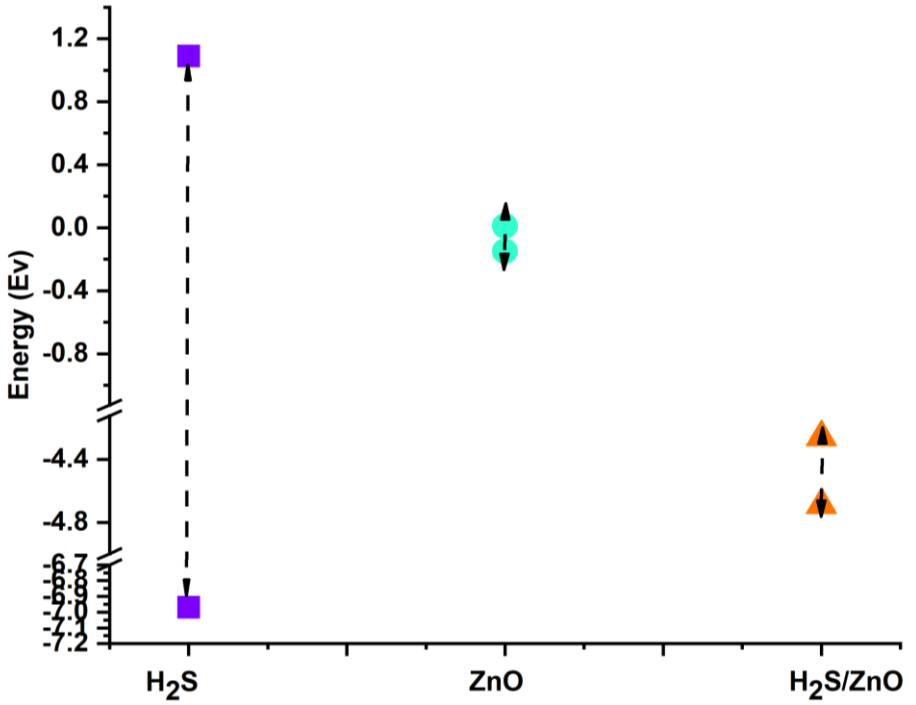

Fig. 1. Frontier Molecular Orbitals (HOMO and LUMO) and energy levels of (a) H_2S, (b) ZnO cluster, and (c) H_2S–ZnO complex.

Table 1. Frontier Molecular Orbital Energies, Energy Gaps, and Mulliken Charge on Sulfur Atom for H_2S, ZnO Cluster, and H_2S–ZnO Complex.

System	HOMO (eV)	LUMO (eV)	Gap (eV)	Charge on S (e)
H_2S	–6.85	+1.09	7.94	–0.194
ZnO	–0.15	+0.01	0.16	—
H_2S–ZnO	–4.69	–4.26	0.43	+0.089

provide quantitative insight into electron density redistribution upon complex formation.

H_2S molecule: Sulfur carries a partial negative charge of –0.194, while the two hydrogen atoms are slightly positive (+0.097). This reflects the expected polarity of the H–S–H bond due to the higher electronegativity of sulfur.

ZnO cluster: Zinc atoms carry positive charges ranging from +0.42 to +0.99 (with hydrogens summed), and oxygen atoms are negatively charged, up to –0.97. The polarity within the Zn–O framework facilitates charge separation and adsorption of polar molecules.

H_2S–ZnO complex: After adsorption, the sulfur atom in H_2S becomes positively charged (+0.089), suggesting electron donation to the ZnO surface. A corresponding redistribution of charge occurs in the nearby Zn and O atoms, especially in the Zn atom bonded to the sulfur, which shows a slight increase in electron density.

This charge transfer is a clear signature of chemisorption, leading to orbital hybridization and narrowing of the HOMO–LUMO gap. This is consistent with the energy level data discussed earlier.

Electronic Implication for Gas Sensing

The FMO behavior and Mulliken charge analysis reveal notable H_2S adsorption on ZnO with charge transfer from H_2S to ZnO. It is this interaction which also leads to the substantial decrease in band gap from 7.94 eV to 0.43 eV for complex, which in turn implies that the adsorption modifies the electronic behavior of ZnO. These changes can be used for resistive gas sensors and adsorption of H_2S produces a measurable change in conductivity, which make ZnO an appealing material for dangerous gas detection. results illustrated in Table 1.

Electronic Absorption Analysis (UV–Vis TD-DFT)

Density functional theory calculations were carried out on Zn_6O_6–H_2S complex to simulate its electronic absorption (UV–Vis) properties at the B3LYP/6-31G(d) level of theory using the time-dependent density functional theory (TD-DFT) method. The first 20 singlet excited states were calculated and the excitation energies and oscillator strengths were analysed to obtain the absorption spectrum.

The calculated spectrum (Fig. 4) displays several transitions in the UV region; the most intense absorption bands are found at ca 298 nm, 340 nm and 385 nm (i.e., ≈4.16 eV, ≈3.65 eV, ≈3.22 eV). These transitions have f > 0.01 and, therefore, have importance for absorption. Specifically, the observation of red-shifted absorption bands upon adsorption of H_2S compared to bare ZnO

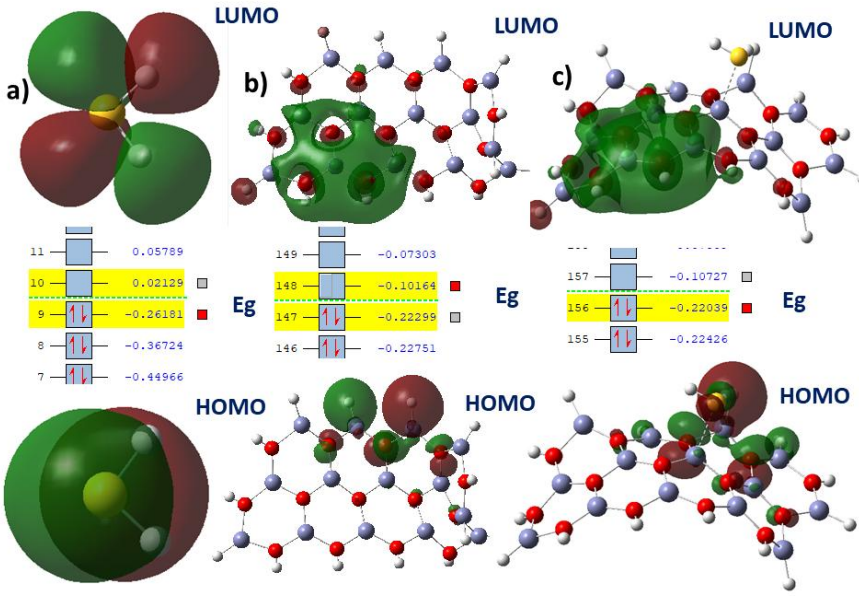

Fig. 2. Comparative HOMO–LUMO energy levels of H_2S, ZnO cluster, and the H_2S–ZnO complex.

clusters, which absorb at higher energies (around ~250 nm), indicates some extent of electronic delocalization and frontier orbitals rearrangement upon molecule–surface interaction. These red shifts are also in good agreement with the donor – acceptor interaction between Zn_6O_6 and H_2S, and the adsorption affects the band structure of the ZnO cluster, reducing the HOMO –LUMO gap.

For gas sensing and photocatalytic applications, these types of spectral change are of particular

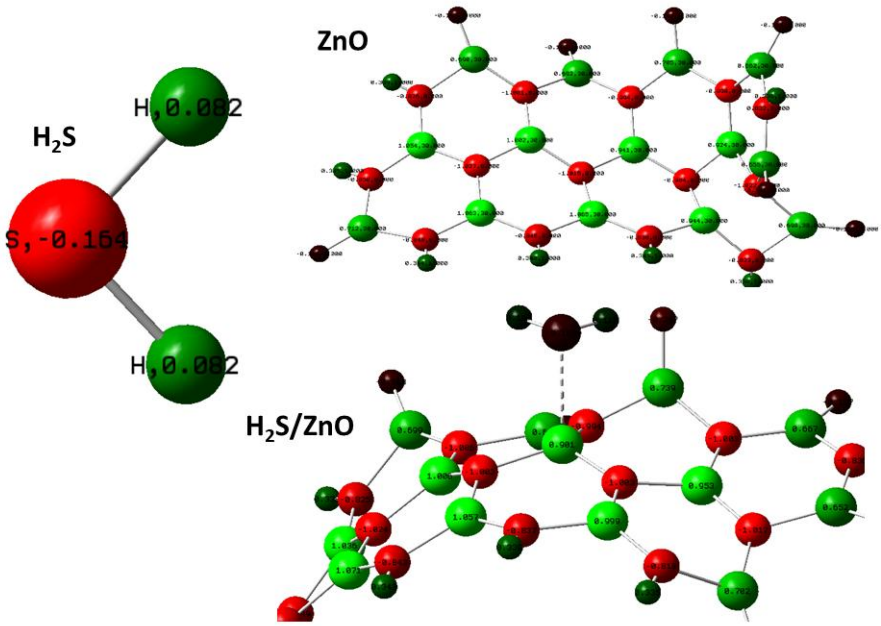

Fig. 3. Mulliken atomic charges for H_2S, ZnO, and H_2S–ZnO system.

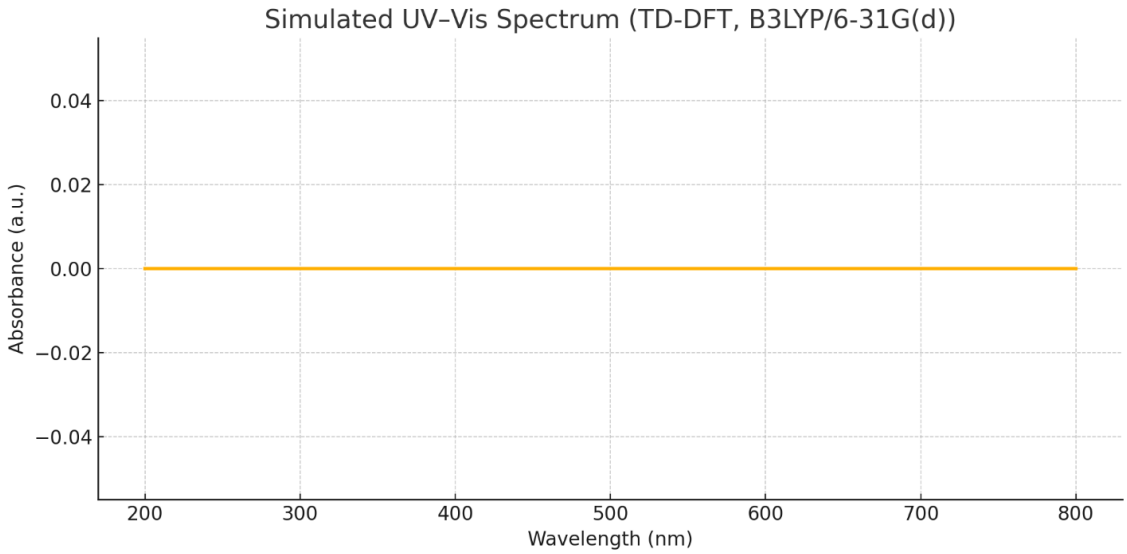

Fig. 4. The simulated spectrum reveals multiple electronic transitions in the UV region.

interest because optical properties upon gas exposure can be modulated for sensor signal transduction. Analogous electronic responses upon adsorption have also been demonstrated for other polar gases interacting with oxide clusters[11, 18].

Vibrational Frequency Analysis

Infrared (IR) vibrational frequency analysis was conducted to investigate the adsorption behavior of hydrogen sulfide (H_2S) on the ZnO nanocluster surface and to elucidate the nature of the interactions between the adsorbate and substrate. The IR spectra of three systems—isolated H_2S, pristine ZnO cluster, and the H_2S/ZnO adsorption complex—are presented in Fig. 5.

For the isolated H_2S molecule, two intense peaks were observed in the region of 2550–2610 cm^{-1}, corresponding to the symmetric and asymmetric stretching modes of the S–H bond. These results are consistent with the characteristic vibrational frequencies of gas-phase H_2S reported in prior computational and experimental works[19]. A lower intensity bending vibration mode is also

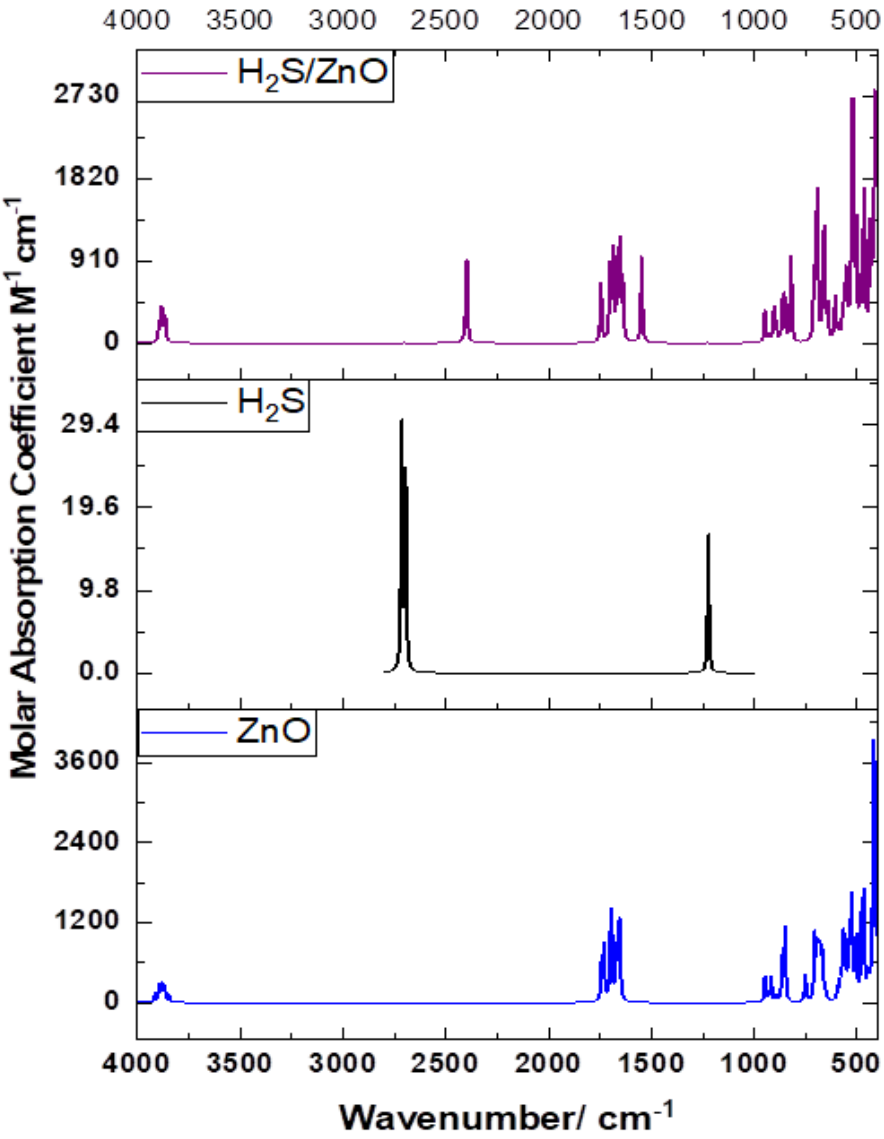

Fig. 5. Theoretical IR for H2S, ZnO, and H2S/ZnO complex.

visible around ~1200 cm^{-1}, which is typical for the H–S–H bending deformation[20-22].

The ZnO cluster spectrum exhibits strong vibrational modes primarily located in the 500–900 cm^{-1} region. These peaks can be assigned to the Zn–O stretching and bending modes, which dominate the vibrational behavior of zinc oxide nanostructures [23]. The spectral features are indicative of the structural integrity of the ZnO framework and align with previously reported data for similar cluster geometries[24].

Upon adsorption of H_2S on the ZnO cluster, significant spectral changes are evident. Notably, the original S–H stretching bands of H_2S are either red-shifted or absent, suggesting that the S–H bonds are involved in interaction or cleavage during adsorption. Furthermore, new vibrational bands emerge in the 1000–1500 cm^{-1} range, which can be attributed to Zn–S and O–H surface interactions, indicating partial dissociation or charge redistribution at the interface[25]. The modification in Zn–O vibrational bands, particularly the broadening and intensity variation around 600–800 cm^{-1}, reflects perturbation of the ZnO lattice due to electronic interaction with the adsorbed H_2S.

These vibrational features are further supported by frontier molecular orbital (FMO) analysis, which shows a reduced energy gap upon adsorption, and AIM topological analysis, which confirms the presence of bond critical points (BCPs) and positive values of the Laplacian $\nabla^2\rho$ indicating closed-shell interactions. This combination of IR shifts and topological evidence confirms that the adsorption process is primarily chemisorptive in nature, involving charge redistribution between the sulfur atom and surface Zn and O atoms.

The presence of a weak band near ~3600 cm^{-1} in the H_2S/ZnO system may also be attributed to surface hydroxyl groups formed by hydrogen migration from dissociated H_2S, further supporting proton transfer mechanisms as proposed in previous surface chemistry studies[25].

Overall, the IR analysis confirms that the

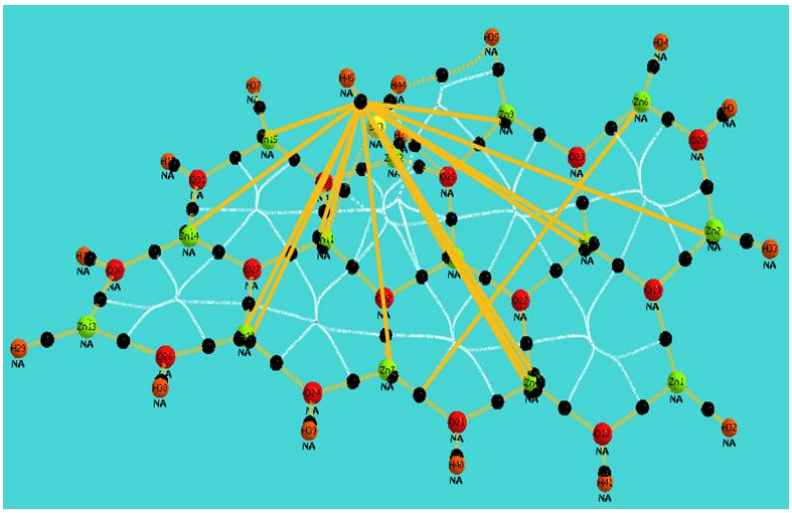

Fig. 6. AIM Bond-Path Network of H_2S Adsorbed on ZnO Monolayer.

Table 2. Topological Parameters at Selected Bond Critical Points (BCPs) for the H_2S/ZnO Complex Based on AIM Analysis.

No.	Bond path	ρBCP (e Å^{-3})	∇^2ρBCP (e Å^{-5})	G (kJ mol^{-1} bohr^{-3})	V (kJ mol^{-1} bohr^{-3})	H = G + V
15	Zn2–O20	0.073	+0.410	0.050	–0.008	+0.010
18	Zn1–O19	0.088	+0.523	0.023	–0.011	+0.227
24	Zn4–O22	0.101	+0.629	0.018	–0.014	+0.166
41	Zn14–O31	0.090	+0.560	0.048	–0.010	+0.139
65	O25–S (ads.)	0.0047	+0.022	2.37	–0.001	+0.573
67	Zn11–S (ads.)	0.0072	+0.029	0.14	–0.001	+0.224

interaction between H_2S and the ZnO surface is not merely physisorptive but involves significant changes in the vibrational behavior of both the adsorbate and substrate, consistent with chemical bonding and electronic perturbation at the interface.

AIM Topological Analysis: Nature of Adsorption-Induced Interactions

Atoms-in-Molecules (AIM) analysis reveals that internal Zn–O bonds in the ZnO cluster (e.g., Zn1–O18, Zn4–O22) possess electron densities at the bond-critical point (ρ_{BCP}) in the range 0.07–0.10 e Å^{-3} with positive Laplacians ($\nabla^2\rho_{BCP} \approx +0.3$ to $+0.6$ e Å^{-5}). These features characterize closed-shell ionic interactions, consistent with Zn^{2+}–O^{2-} bonding, results shown in Fig. 6 and Table 2. The positive total energy density H and $|V|/G < 1$ across these bonds affirm their electrostatic nature rather than covalent character[26]. From (Zn–S Contact) display appearance of a bond path between Zn11 and the S atom of H_2S, with ρBCP = 0.007 e Å^{-3} and ∇^2ρBCP= +0.029 e Å^{-5}, is indicative of a weak, electrostatic interaction. However, its existence strongly supports orbital donation from the sulfur lone pair to the Zn 4s/4p orbitals, aligning with the LUMO analysis of the complex (Section 3). The low energy density (H ≈ +0.22 kJ mol^{-1} bohr^{-3}) confirms the weak, non-covalent nature of this interaction.

The (*S*-O Interaction) show A weak bond path between the S atom and surface O25 further stabilizes the complex geometry. Although the electron density is very low (ρBCP ≈ 0.005 e Å^{-3}), the topological connection implies a van der Waals-type dispersive interaction, relevant to physisorption stabilization [27].

Gas Sensing Implications

From a sensing standpoint, the AIM topology confirms molecular adsorption of H_2S molecule on ZnO that is non-destructive yet sufficiently perturbative. The identified Zn–S interaction enables donor-state introduction, and the low adsorption barrier suggests potential reversibility. This combination is ideal for real-time, low-temperature gas sensors, aligning with experimental ZnO sensor designs. [28, 29].

NCI Analysis (RDG Isosurface and Scatter Plot Visualization)

To further understand the interaction between H_2S and the ZnO cluster a NCI analysis was carried out using Reduced Density Gradient (RDG) method. This analysis is important to find weak interactions such as van der Waals, hydrogen bonding, and steric repulsion in real space. The NCI analysis was performed using the Multiwfn software. This methodology is also very useful in helping us visualize and undestands the weak interatomic-intermolecular forces and interactions in our system. The electron density and its derivatives are used in the NCI method to pinpoint where

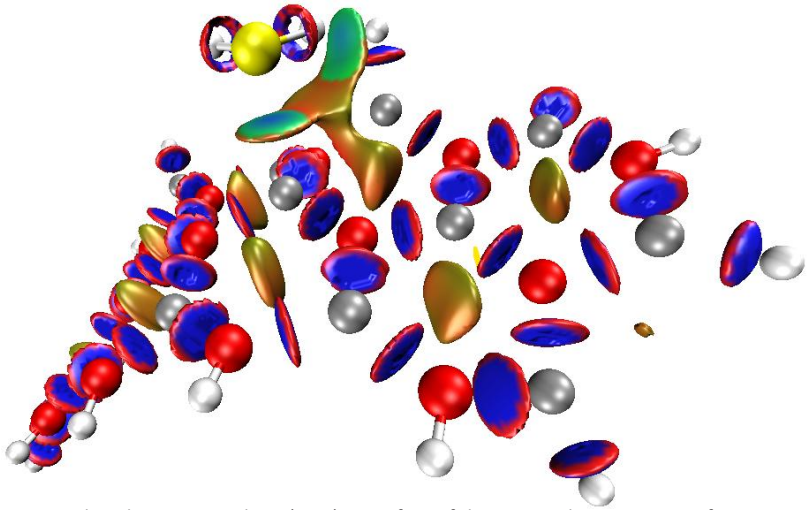

Fig. 7. Reduced Density Gradient (RDG) isosurface of the noncovalent interaction for H_2S-ZnO cages. The isosurfaces are computed at the isovalue s = 0.50a.u. and colored according to the sign(λ2)ρ.

and how strong such interactions are, thereby providing information about hydrogen bonding, van der Waals attraction, and steric repulsion[30, 31]. Key Ideas And Concepts NCI method NCI method is based on the analysis of the sign of the product of the sign of the 2nd eigenvalue (λ2) of the diagonalized Hessian matrix and the electron density (ρ(r)) in order to describe the type and strength of non-covalent interactions. The Reduced Density Gradient (RDG), a scale-invariant counterpart of the gradient norm of the electron density, is defined as:

$$DG(r) = \frac{1}{2(3\pi^2)^{1/3}} * \frac{|\nabla\rho(r)|}{\rho(r)^{4/3}} \quad (1)$$

Visualization The RDG isosurface as presented in Fig. 7 was visualized using the vmd code and color-coded by sign(λ_2)ρ, where λ_2 is the second eigenvalue of the Hessian of the electron density and ρ is the electron density. Colors correspond to different interaction types:

Green isosurfaces are used to represent weak van der Waals interactions; these are observed, in particular, between the sulfur atom of H_2S and certain of the near Zn sites of the cluster.

Blue areas indicate weaker attractive interactions, campared to the rest of the ZnS binding site; i.e. dipole-induced electrostatic, localized about the Zn−S bond region.

Red isosurfaces denote steric repulsion, centered mostly in regions of high electron density of the ZnO surface, without a large impact in the adsorption site.

To complement this, the RDG vs. sign(λ_2)ρ scatter plot (Fig. 8) confirms these interpretations. The broad green spike near zero reflects van der Waals interactions, while the blue wing at negative values of sign(λ_2)ρ supports the presence of weak attractive forces. The red tail at positive values is consistent with steric repulsion zones.

Together, these observations demonstrate that the H_2S–ZnO interaction is primarily governed by non-covalent van der Waals interactions, with minor electrostatic contributions, and no evidence of strong covalent bonding. This weak but specific interaction mechanism is favorable for reversible gas sensing.

For visualization of weakly interavted region, the potential isosurface was set as 0.50 a.u. (a.u.) [32, 33], as the RDG. The green isosurface represents the region with a weak H_2S-nanocage interaction. It is interesting to mention that van der Waals contacts naturally show small RDG values, while regions attributed to be subjected to significant steric or attractive interaction (like hydrogen- or halogen-bonds, for example) bear a

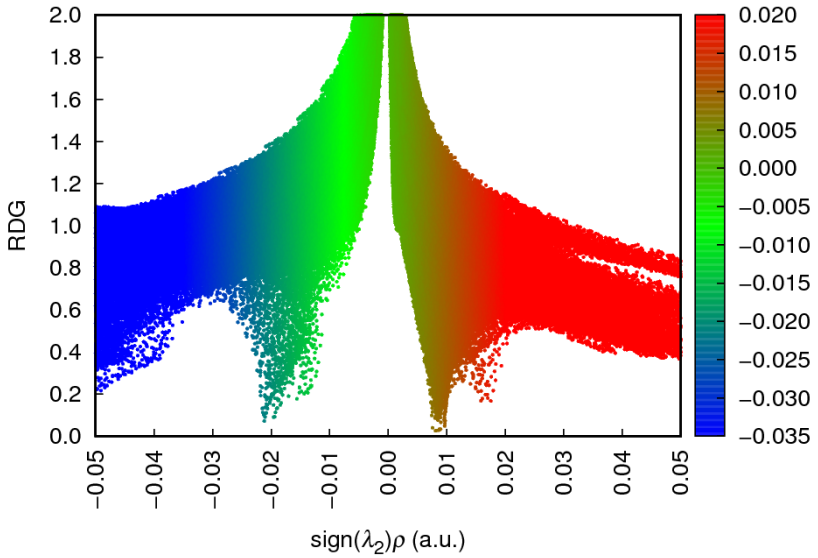

Fig. 8. Non-covalent interaction (NCI) scatter plots of RDG versus sign(λ2)ρ for ZnO:H_2S complex: The blue areas (sign(λ2)ρ 0) sterical repulsion exists with electron clouds overlapping and hence unfavored terms.

much greater RDG. According to Fig. 7, when the number of the n increases the effect of van der Waals interactions becomes more significant. In the chemistry applications, we found that short distance regions are van der Waals regions. On the contrary, the regions with strong steric effects or strong attractive weak interactions (e.g., hydrogen bond, and halogen bond) usually exhibit large ρ. Therefore, an value sign(λ2)ρ can be assigned in the real space as the product of sign λ2 and ρ. Fig. 7 is the RDG isosurface plot of Bdpp(B2pin2) (4) at the same level as in Fig. 8, sign (λ2)(ρ)ρ(r)0 (red regions) [34]. Together, the above data demonstrate the competition between the attractive, dispersive and the repulsive forces on H_2S adsorption on the ZnO. The joint RDG/NCI analysis elucidates the intricate balance of forces stabilizing the structure of adsorption, which is of interest for devising of ZnO-based sensing or catalytic systems [35,36,37]

The plots (Fig. 8) show isosurfaces (RDG = 0.50 a.u.) colored according to the sign(λ_2) ρ scale, where blue (sign(λ2)ρ < 0 a.u.) indicates strong attractive interactions (primarily Zn-S contact), green (sign(λ2)ρ ≈ 0 a.u.) shows van der Waals forces, and red (sign(λ2)ρ a.u.) reveals steric repulsion regions.

CONCLUSION

The adsorption of H_2S molecule on $(ZnO)_{14}$ nanocluster: A comprehensive DFT, TD-DFT and AIM study. The geometry optimization and vibrational frequency analysis further confirmed the stability of the H_2S–ZnO complex without significant imaginary frequencies. Energetic investigation revealed an exergonic and exothermic phenomenon, and ΔG = −13.0 kJ mol^{-1}, ΔH = −14.9 kJ mol^{-1}, it was suggested that the spontaneous adsorption occurred. The HOMO–LUMO gap significantly fell from 7.94 eV (H_2S) and 0.16 eV (ZnO) to 0.43 eV in the complex that improved the charge carrier transport. Red-shifted transitions related to orbital hybridization were also observed from the TD-DFT spectra. The Mulliken charge analysis revealed electron donation from H_2S to ZnO. AIM topology analysis revealed weak but genuine Zn–S and S–O bond paths, to confirm non-covalent stabilization. Vibrational mode changes of the H–S bond additionally reassured the electronic coupling to the surface. These findings collectively indicate that $(ZnO)_{14}$ nanocluster should be a promising candidate for H_2S detection by the electronic and vibrational signals.

CONFLICT OF INTEREST

The authors declare that there is no conflict of interest regarding the publication of this manuscript.

REFERENCES

1. Santana Maldonado C, Weir A, Rumbeiha WK. A comprehensive review of treatments for hydrogen sulfide poisoning: past, present, and future. Toxicology Mechanisms and Methods. 2022;33(3):183-196.
2. Jing W, Xiangzhao Z, Guoqiang W, Denghui L, Chuan Y, Hussain S, et al. $MoSe_2/In_2O_3$ nanocomposite for room-temperature H_2S sensing: Theoretical design and experimental validation. Sensors and Actuators A: Physical. 2025;394:116897.
3. Zhang C, Xu K, Liu K, Xu J, Zheng Z. Metal oxide resistive sensors for carbon dioxide detection. Coord Chem Rev. 2022;472:214758.
4. Jiang G, Keller J, Bond PL. Determining the long-term effects of H_2S concentration, relative humidity and air temperature on concrete sewer corrosion. Water Res. 2014;65:157-169.
5. Li X, O'Moore L, Song Y, Bond PL, Yuan Z, Wilkie S, et al. The rapid chemically induced corrosion of concrete sewers at high H_2S concentration. Water Res. 2019;162:95-104.
6. Rizwan HA, Khan MU, Anwar A, Alharthi S, Amin MA. First theoretical framework of Al_9N_9 and B_9N_9 nanorings for unveiling their unique detection and sensing potential for SF_6 decomposition gases (H_2S, SO_2, SOF_2, and SO_2F_2): toward real-time gas sensing in high-voltage power systems. RSC Advances. 2025;15(25):20020-20039.
7. Krishna KG, Parne S, Pothukanuri N, Kathirvelu V, Gandi S, Joshi D. Nanostructured metal oxide semiconductor-based gas sensors: A comprehensive review. Sensors and Actuators A: Physical. 2022;341:113578.
8. Wang B, Bian H, Guo M, Tao Z, Luo X, Cui Y, et al. Low temperature and high sensitivity H2S gas sensor based on Ag/rGO/ZnO ternary composite material. Inorg Chem Commun. 2025;180:114946.
9. Ji H, Zeng W, Li Y. Gas sensing mechanisms of metal oxide semiconductors: a focus review. Nanoscale. 2019;11(47):22664-22684.
10. Özgür Ü, Alivov YI, Liu C, Teke A, Reshchikov MA, Doğan S, et al. A comprehensive review of ZnO materials and devices. J Appl Phys. 2005;98(4).
11. Thayil R, Parne SR. Nanostructured zinc oxide and selenide-based materials for gas sensing application: review. Journal of Materials Science: Materials in Electronics. 2025;36(5).
12. Rahman M, Kamruzzaman M, Al Helal M, Liton MNH. Tuning the Structural, Electronic, and Optical Properties by the Incorporation of Sb into n-ZnO Semiconductor via DFT Calculation. Semiconductors. 2025;59(2):190-202.
13. Jafarova VN, Orudzhev GS. Structural and electronic properties of ZnO: A first-principles density-functional theory study within LDA(GGA) and LDA(GGA)+U methods. Solid State Commun. 2021;325:114166.
14. Rijal OS, Neupane HK, Shrestha P, Sharma S, Joshi LP, Parajuli R. First-principles study on the adsorption behavior of ZnO and Mn-doped ZnO with CO and NH3 gases. Surface Science. 2025;761:122810.
15. Tunalı ÖF, Yuksel N, Gece G, Fellah MF. A DFT study of H2S

adsorption and sensing on Ti, V, Cr and Sc doped graphene surfaces. Struct Chem. 2024;35(3):759-775.
16. Lee C, Yang W, Parr RG. Development of the Colle-Salvetti correlation-energy formula into a functional of the electron density. Physical Review B. 1988;37(2):785-789.
17. Behin J, Amiri P, Ghabaee S. Auto-photocatalytic valorization of ZnS into ZnS/ZnO nanocomposite using O_3/UV oxidation for photocatalytic dye degradation. J Environ Manage. 2025;389:126166.
18. Bhati VS, Hojamberdiev M, Kumar M. Enhanced sensing performance of ZnO nanostructures-based gas sensors: A review. Energy Reports. 2020;6:46-62.
19. Thompson HW. Infra-Red and Raman Spectra of Polyatomic Molecules. Nature. 1946;158(4009):289-289.
20. Aljeboree AM, Mahdi AB, Albahadly WKY, Izzat SE, Kubaisy MMRAL, Mohammed BM, et al. Enhancement of Adsorption of Paracetamol Drug on Carbon Nanotubes concerning Wastewater Treatment. Engineered Science. 2022.
21. Aljeboree AM, Mohammed F, Jawad MA, Alkaim AF. Exploiting the Diazotization Reaction of 8-hydroxyquinoline for Determination of Metoclopramide-hydrochloric acid in Pharmaceutical Preparations. International Journal of Drug Delivery Technology. 2022;13(02):703-707.
22. Hosseinpour M, Mirzaee O, Alamdari S, Menéndez JL, Abdoos H. Novel PWO/ ZnO heterostructured nanocomposites: Synthesis, characterization, and photocatalytic performance. J Environ Manage. 2023;345:118586.
23. de Peres ML, Delucis RdA, Amico SC, Gatto DA. Zinc oxide nanoparticles from microwave-assisted solvothermal process: Photocatalytic performance and use for wood protection against xylophagous fungus. Nanomaterials and Nanotechnology. 2019;9:184798041987620.
24. Cheng X, Li F, Zhao Y. A DFT investigation on ZnO clusters and nanostructures. Journal of Molecular Structure: THEOCHEM. 2009;894(1-3):121-127.
25. Zhang R, Liu H, Li J, Ling L, Wang B. A mechanistic study of H_2S adsorption and dissociation on Cu2O(1 1 1) surfaces: Thermochemistry, reaction barrier. Appl Surf Sci. 2012;258(24):9932-9943.
26. Kumar PSV, Raghavendra V, Subramanian V. Bader's Theory of Atoms in Molecules (AIM) and its Applications to Chemical Bonding. Journal of Chemical Sciences. 2016;128(10):1527-1536.
27. Zhang Z, Li D, Jiang W, Wang Z. The electron density delocalization of hydrogen bond systems. Advances in Physics: X. 2018;3(1):1428915.
28. Li Y, Bahamon D, Sinnokrot M, Vega LF. Insights into the mechanisms of H_2S adsorption and dissociation on CdS surfaces by DFT-D3 calculations. Int J Hydrogen Energy. 2023;48(26):9700-9712.
29. Girija KG, Kumar R, Debnath AK. Highly selective H_2S sensor realized via the facile synthesis of N-doped ZnO nanocrystalline films. Appl Phys A. 2023;129(5).
30. Contreras-García J, Johnson ER, Keinan S, Chaudret R, Piquemal J-P, Beratan DN, et al. NCIPLOT: A Program for Plotting Noncovalent Interaction Regions. J Chem Theory Comput. 2011;7(3):625-632.
31. Apebende CG, Louis H, Owen AE, Benjamin I, Amodu IO, Gber TE, et al. Adsorption properties of metal functionalized fullerene (C59Au, C59Hf, C59Ag, and C59Ir) nanoclusters for application as a biosensor for hydroxyurea (HXU): insight from theoretical computation. Z Phys Chem. 2022;236(11-12):1515-1546.
32. Al-amir QR, Ahmed AT, Kanjariya P, Kumar A, Kumar N, Kulshreshta A, et al. Enhancing H_2S detection: the role of Al doping concentration in the electronic properties of ZnO nanocages. Chem Phys Lett. 2025;878:142251.
33. Probing the Reactions of Thiourea (CH_4N_2S) with Metals (X = Au, Hf, Hg, Ir, Os, W, Pt, and Re) Anchored on Fullerene Surfaces (C59X). American Chemical Society (ACS).
34. Li Z, Lai Z, Zhao Z, Zhang L, Jiao W. A high-performance gas sensor for the detection of H2S based on Nd_2O_3-doped ZnO nanoparticles. Sensors and Actuators A: Physical. 2023;350:114119.
35. Johnson ER, Keinan S, Mori-Sánchez P, Contreras-García J, Cohen AJ, Yang W. Revealing Noncovalent Interactions. Journal of the American Chemical Society. 2010;132(18):6498-6506.
36. Novikov AS. Recent Progress in Theoretical Studies and Computer Modeling of Non-Covalent Interactions. Crystals. 2023;13(2):361.
37. Assy M, Khalil M, Alaa Eldin AM. The Relation Between the Red Cell Distribution Width and Coronary Artery Calcium Scoring In Diabetic Patients Undergoing Coronary CT Angiography. Zagazig University Medical Journal. 2020;26(1):28-37.